Locally and globally optimal configurations of N particles on the sphere with applications in the narrow escape and narrow capture problems

Wesley J. M. Ridgway* and Alexei F. Cheviakov†
Department of Mathematics and Statistics, University of Saskatchewan, Saskatoon, Saskatchewan S7N 5E6, Canada

(Received 13 December 2018; revised manuscript received 5 August 2019; published 28 October 2019)

Determination of *optimal* arrangements of N particles on a sphere is a well-known problem in physics. A famous example of such is the Thomson problem of finding equilibrium configurations of electrical charges on a sphere. More recently, however, similar problems involving other potentials and nonspherical domains have arisen in biophysical systems. Many optimal configurations have previously been computed, especially for the Thomson problem; however, few results exist for potentials that correspond to more applied problems. Here we numerically compute optimal configurations corresponding to the *narrow escape* and *narrow capture* problems in biophysics. We provide comprehensive tables of global energy minima for $N \leqslant 120$ and local energy minima for $N \leqslant 65$, and we exclude all saddle points. Local minima up to $N = 120$ are available online.

DOI: 10.1103/PhysRevE.100.042413

I. INTRODUCTION

The problem of optimally distributing N points on the boundary of a bounded domain, $\mathcal{D} \subseteq \mathbb{R}^n$ ($n \geqslant 2$), has many applications in physical systems (see, e.g., Ref. [1] and numerous references therein). Here, *optimal* refers to an arrangement of points, particles, etc., on the boundary, $\partial\mathcal{D}$, such that the configuration of particles $\{\mathbf{x}_i\}_{i=1}^N$ minimizes the pairwise "potential energy"

$$\mathcal{H}(\mathbf{x}_1, \ldots, \mathbf{x}_N) = \sum_{i<j}^{N} h(|\mathbf{x}_i - \mathbf{x}_j|) \tag{1}$$

with the constraint $\mathbf{x}_i \in \partial\mathcal{D}$, where h is the interaction energy between two particles. Such a configuration is called an *optimal configuration*. Note that optimal configurations include local minima of (1) as well as the global minimum. While a large number of algorithms have been used to seek global extrema of general or specific classes of functions [2–5], very few algorithms exist for the study of local minima [6]. A large part of this paper is devoted to systematic computations of *local* minima which presents a difficult computational problem due to the number of local minima. In fact, it is believed that the number of local minima increases exponentially with N [6].

One example of a problem of practical interest that yields the above-described optimization problem is the *narrow escape problem* in which a Brownian particle diffuses in a bounded domain $\Omega \subset \mathbb{R}^n$ ($n \geqslant 3$). The boundary $\partial\Omega = \partial\Omega_a \cup \partial\Omega_r$ consists of reflecting and absorbing regions, denoted $\partial\Omega_r$ and $\partial\Omega_a$, respectively, where the absorbing regions are small windows or traps with measure $|\partial\Omega_a| = O(\epsilon^{n-1})$, $0 < \epsilon \ll 1$. The narrow escape problem consists of finding the mean first passage time (MFPT), defined as the expectation value of the time required for the Brownian particle to escape Ω through $\partial\Omega_a$ in the limit where ϵ is asymptotically small. The narrow escape problem is a singular perturbation problem since the MFPT diverges in the limit as $\epsilon \to 0$ [7,8].

When $n = 3$ and the absorbing boundary consists of N disjoint circular caps of a common (dimensionless) radius ϵ, $\partial\Omega_{\epsilon_i}$, $i = 1, \ldots, N$, the MFPT, $v(x)$, satisfies the boundary value problem

$$\Delta v = -\frac{1}{D}, \quad x \in \Omega, \quad v = 0, \quad x \in \partial\Omega_a = \bigcup_{i=1}^{N} \partial\Omega_{\epsilon_i},$$
$$\partial_n v = 0, \quad x \in \partial\Omega_r, \tag{2}$$

where D is the diffusivity of the Brownian motion. The situation is depicted in Fig. 1. We remark that in 2D a heterogeneous Dirichlet-Neumann problem is also known as the *Keldysh-Sedov problem*, originally considered for the Laplace equation (see, e.g., Refs. [9,10]).

The average MFPT for a uniform distribution of starting locations for the Brownian particle is computed from

$$\bar{v} = \frac{1}{|\Omega|} \int_{\Omega} v(x) dx, \tag{3}$$

where $|\Omega|$ is the volume of Ω.

The narrow escape problem has application in biophysics where proteins, ions, etc. (modeled as Brownian particles), diffuse in a confining domain. Specific examples include virus transport inside cell nuclei, chemical reactions in microdomains, and the motion of calcium ions in dendritic spines (see Refs. [11,12] and references therein). As there are usually many Brownian particles, the average MFPT, (3), acts as a timescale for these particles to exit the domain to accomplish some biological function. A natural problem arising out of this model is that of computing arrangements of traps that minimize the average MFPT. This constitutes a constrained optimization problem in which the objective

*Corresponding author: wjr704@mail.usask.ca
†cheviakov@math.usask.ca

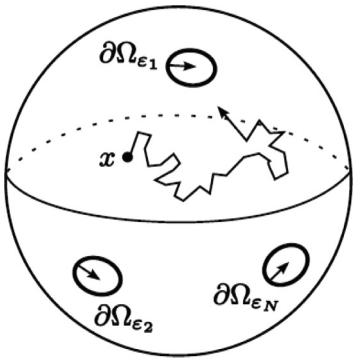

FIG. 1. Illustration of Brownian motion in a sphere with absorbing patches on an otherwise reflecting boundary corresponding to the BVP (2).

function is of the form (1) and will be discussed in greater detail in the next section.

Another specific example is the *narrow capture problem*, similar to the narrow escape problem, which also has applications in biophysics (see Refs. [13,14] and references therein). Here, there are M disjoint interior absorbing traps, $\Omega_\epsilon \subset \Omega$, each with a size parameter $\epsilon \ll 1$, and the boundary of Ω is entirely reflecting [15]. The case where $\Omega \subset \mathbb{R}^3$ contains a single spherical trap ($M = 1$) of radius ϵ centered at $\mathbf{x}_0 \in \Omega$ was studied in Ref. [14]. The boundary of the target sphere is reflecting except for N disjoint circular absorbing nanotraps of a common radius, σ. That is, $\partial\Omega_\epsilon = \partial\Omega_{\epsilon_r} \cup \partial\Omega_{\epsilon_a}$, where $\partial\Omega_{\epsilon_a}$ and $\partial\Omega_{\epsilon_r}$ are the absorbing and reflecting regions, respectively. The situation is depicted in Fig. 2. The MFPT $v(x)$ for a Brownian particle starting at $x \in \Omega\backslash\Omega_\epsilon$ satisfies the boundary-value problem

$$\begin{aligned} &\Delta v = -\frac{1}{D}, \quad x \in \Omega\backslash\Omega_\epsilon, \quad v = 0, \quad x \in \partial\Omega_{\epsilon_a}, \\ &\partial_n v = 0, \quad x \in \partial\Omega \cup \partial\Omega_{\epsilon_r}. \end{aligned} \tag{4}$$

The average MFPT is computed using (3) but replacing Ω with $\Omega\backslash\Omega_\epsilon$.

The narrow capture problem models some biophysical processes. For example, a cell transports proteins (again modeled by Brownian particles) between the cytoplasm and the cell nucleus which is roughly spherical in shape. Proteins are allowed to pass through the otherwise impermeable nuclear membrane via nuclear pore complexes (NPCs) distributed over the surface. There are nearly 2000 of these pores covering about 2% of the nuclear surface; each has a radius of about

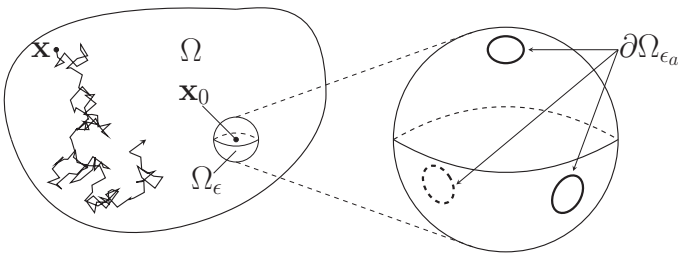

FIG. 2. Illustration of the narrow capture problem consisting of a single target sphere with absorbing patches inside a general domain.

25 nm [14]. The average MFPT again provides a timescale for the large number of particles to escape the domain to accomplish a biological function.

Another practical problem is modeling the diffusion of nanoparticles in so-called inverse opals. Inverse opals are porous materials consisting of connected spherical cavities. These materials have several applications in engineering and are interesting from a materials science perspective (see, e.g., Refs. [16,17] and references therein). Although diffusion in these structures has been studied experimentally and numerically (see, e.g., Ref. [18]), development of a general model of the diffusion process that takes into account the geometric structure is an open problem. The MFPT for a spherical cavity with pores may provide a measure of the average "dwell" time of a particle in each cavity. One would expect optimal configurations to maximize the diffusion which is desirable when designing materials for industrial processes. Thus the narrow escape problem and corresponding optimal configurations are relevant in the modeling of this problem.

Optimal configurations on the sphere in $\mathbb{R}^3$ for the general pairwise potential (1), where h in (1) is a continuous and monotonically decreasing function, have previously been studied (e.g., Refs. [19,20]). It is well known that the optimal configurations depend on the potential for all N with a few exceptions ($N = 2, 3, 4, 6, 12$). The global minima for these N are optimal for every such h and these configurations are termed *universally optimal*. The universal optima in $\mathbb{R}^3$ consist of antipodal points ($N = 2$), an inscribed equilateral triangle ($N = 3$), a tetrahedron ($N = 4$), an octahedron ($N = 6$), and an icosahedron ($N = 12$). This is a complete list for $\mathbb{R}^3$ [20].

It is also well known that it is geometrically impossible, in general, to evenly distribute points on a sphere. If c_i is the coordination number (number of nearest neighbors) of particle i, then the Euler formula for the sphere yields (e.g., [1])

$$\sum_{i=1}^{N}(6 - c_i) = 12, \tag{5}$$

which shows that the total defect structure must always be 12. For example, a tessellation of the sphere with hexagons and pentagons must always contain exactly 12 pentagons. Our results are consistent with these facts. In light of Eq. (5), we define a *scar* as a collection of adjacent defects.

In this paper we compute local and global minima of some selected potentials that have applications in the narrow escape and narrow capture problems up to $N = 120$. The rest of the paper is organized as follows: First we summarize the results of Refs. [8,14] and present the potentials that we will consider (Sec. II). Then in Sec. III we describe briefly the optimization algorithm [21]. The remaining sections present the results with comprehensive tables of local and global minima as well as interpretation and comparison with previous work [22].

II. ASYMPTOTIC FORMULAS FOR THE AVERAGE MFPT AND RELATED OPTIMIZATION PROBLEMS

The narrow escape problem for the unit sphere with N identical "circular" traps of radius $\epsilon \ll 1$ was studied in

[8]. The MFPT was computed using the method of matched asymptotic expansions using information about the surface Neumann Green's function for the sphere. It was shown that the average MFPT has the following asymptotic series, accurate to $O(1)$:

$$\bar{v} = \frac{|\Omega|}{4\epsilon DN}\left\{1 + \frac{\epsilon}{\pi}\log\left(\frac{2}{\epsilon}\right) + \frac{\epsilon}{\pi}\left[-\frac{9N}{5} + 2(N-2)\log 2 + \frac{3}{2} + \frac{4}{N}\mathcal{H}_{\rm NE}(x_1,\ldots,x_N)\right] + O(\epsilon^2\log\epsilon)\right\}, \tag{6}$$

where D is the diffusivity of the Brownian motion, $|\Omega|$ is the volume of the unit sphere, and the function $\mathcal{H}_{\rm NE}(x_1,\ldots,x_N)$ is a discrete pairwise energy given by

$$\mathcal{H}_{\rm NE} = \sum_{i<j}^{N}\left[|\mathbf{x}_i - \mathbf{x}_j|^{-1} - \frac{1}{2}\log|\mathbf{x}_i - \mathbf{x}_j| - \frac{1}{2}\log(2 + |\mathbf{x}_i - \mathbf{x}_j|)\right]. \tag{7}$$

The first two terms are the usual Coulombic and logarithmic potentials, respectively,

$$\mathcal{H}_{\rm C} = \sum_{i<j}^{N}|\mathbf{x}_i - \mathbf{x}_j|^{-1}, \tag{8}$$

$$\mathcal{H}_{\rm L} = -\sum_{i<j}^{N}\log|\mathbf{x}_i - \mathbf{x}_j|. \tag{9}$$

Thus the configuration of traps that minimizes the MFPT is obtained by minimizing the discrete pairwise energy (7).

The narrow capture problem for M interior targets was analyzed in Ref. [15] using the method of matched asymptotic expansions in order to arrive at a three-term expansion in ϵ for the MFPT. For a single target ($M = 1$) the result for the average MFPT reduces to

$$\bar{v} = \frac{|\Omega|}{4\pi CD\epsilon}[1 + 4\pi\epsilon\, CR(\mathbf{x}_0) + O(\epsilon^2)], \tag{10}$$

where $R(\mathbf{x}_0)$ is the regular part of the Neumann Green's function for Ω. The quantity C, called the capacitance of the target sphere, is defined in terms of an electrostatic potential problem. When the target sphere consists of a reflecting boundary with absorbing patches as in [14], the capacitance is defined in terms of the boundary-value problem

$$\Delta\phi = 0, \quad \mathbf{y} \in \mathbb{R}^3\backslash\mathcal{B}, \quad \phi = 0, \quad \mathbf{y} \in \Gamma_a,$$
$$\partial_n\phi = 0, \quad \mathbf{y} \in \Gamma_r, \quad \lim_{R\to\infty}\int_{\partial\mathcal{B}_R}\partial_n\phi\, dS = -4\pi, \tag{11}$$

where $\mathcal{B}$ is the magnified target sphere centered at the origin with unit radius and $\mathcal{B}_R$ is a sphere of radius R centered at the origin. The reflecting and absorbing areas on $\mathcal{B}$ are denoted by Γ_r and Γ_a, respectively. The far-field behavior of the solution defines C by

$$\phi \sim \frac{1}{|\mathbf{y}|} - \frac{1}{C}\left[1 - \frac{\mathbf{p}\cdot\mathbf{y}}{|\mathbf{y}|^3}\right] + \cdots \quad \text{as } |\mathbf{y}| \to \infty, \tag{12}$$

where $\mathbf{p}$ is the dipole moment corresponding to the magnified target sphere (cf. Ref. [15]). In Ref. [14] it was shown that the capacitance for the target sphere is given by

$$\frac{1}{C} = \frac{\pi}{N\sigma}\left\{1 + \frac{\sigma}{\pi}\left[\log(2e^{-3/2\sigma}) + \frac{4}{N}\mathcal{H}_{\rm NC}\right] + O\left(\sigma^2\log\left(\frac{\sigma}{2}\right)\right)\right\}. \tag{13}$$

As is the case with the MFPT for the narrow escape problem, $\mathcal{H}_{\rm NC}$ is a discrete energy-like function defined by

$$\mathcal{H}_{\rm NC} = \mathcal{H}_{\rm C} - \frac{1}{2}\mathcal{H}_{\rm L} - \sum_{i<j}^{N}\frac{1}{2}\log(2 + |\mathbf{x}_i - \mathbf{x}_j|). \tag{14}$$

Minimizing $\mathcal{H}_{\rm NC}$ minimizes the average MFPT for the narrow capture problem. Equations (14) and (7) differ only in the sign of $\mathcal{H}_{\rm L}$.

The main focus of this paper is to systematically compute optimal configurations of particles on the sphere that minimize (7) and (14) when $N \leqslant 120$. We will refer to these potentials as the narrow escape (NE) and narrow capture (NC) potentials, respectively. Optimal configurations for the narrow escape potential have previously been computed, but only the global minima [8,22]. In [23] optimal configurations for the narrow escape potential with two differently "charged" particles were computed. Here we attempt to compute all local minima for N identically charged particles in addition to the global minimum. The optimal configurations for the narrow capture potential have not previously been studied.

Optimal configurations for more common potentials, such as the Coulombic (8) and logarithmic (9) potentials, have been studied more extensively [21,24–27]. These potentials also have several physical applications and are used in benchmarking optimization software. For example, the determination of optimal configurations on the sphere for the Coulomb potential (8) constitutes the classic and well-known Thomson problem. The modeling of multielectron bubbles in liquid helium is a modern example of the Thomson problem [28]. The logarithmic potential has applications in the modeling of vortex defects in superconductors [1].

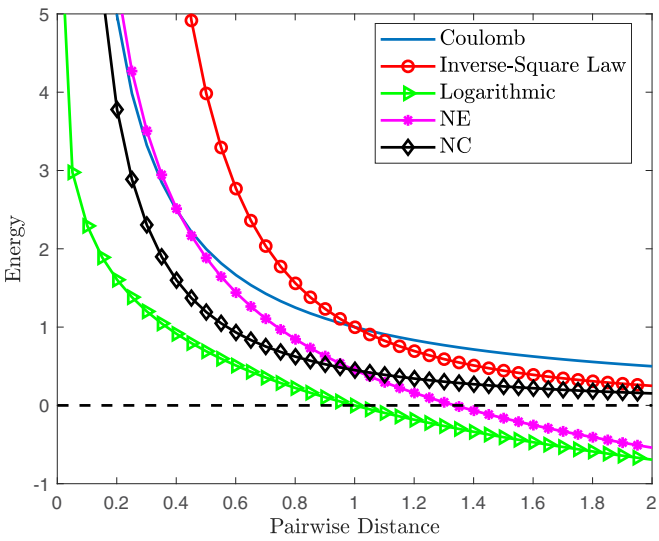

FIG. 3. Pairwise energies for each potential (7)–(9), (14), and (15). Over the unit sphere, the pairwise distance is at most 2.

Optimal configurations for inverse power law potentials relate closely to packing problems. Finding the most efficient packing of spherical caps on the surface of a sphere constitutes the best-packing problem for the sphere, also known as the Tammes problem. The solutions to this problem are given by optimal configurations of a short range power law,

$$\mathcal{H}_m = \sum_{i<j}^{N} \frac{1}{|\mathbf{x}_i - \mathbf{x}_j|^m}, \quad m \to \infty. \tag{15}$$

The case where $m = 2$ was examined numerically in Ref. [21]. Figure 3 compares various potential functions.

III. NUMERICAL COMPUTATION OF OPTIMAL CONFIGURATIONS

In this section, we describe briefly the optimization algorithm employed to compute putatively optimal configurations. Details are given in Ref. [21]. The algorithm consists broadly of three steps:

(1) Generation of initial configurations as starting points for optimization.

(2) Energy minimization via modified steepest descent.

(3) Removal of saddle points.

The algorithm generates N-particle starting configurations by computing a triangulation of previously known $(N-1)$-particle optimal configurations. The Nth particle is inserted at the center of mass of one of the triangles on the convex hull of the triangulation and projected onto the surface of the sphere. This procedure is performed for each triangle center; thus for each triangle center one obtains a starting configuration. Due to the possible symmetry of the $(N-1)$-particle configuration, as well as the rotational and reflection invariance of the energy, some of the resulting starting configurations may be identical. The redundant configurations are identified and excluded by calculating pairwise distances between particles.

Local optimization is accomplished by a modified steepest descent algorithm. Define forces acting on particle i according to

$$\mathbf{F}_i = -\nabla_i \mathcal{H}(\mathbf{x}_1, \ldots, \mathbf{x}_N), \tag{16}$$

where ∇_i is the gradient operator with respect to the coordinates of particle i. At each step of the energy minimization, the position of the ith particle, $\mathbf{x}_i$ is updated according to

$$\mathbf{x}_i \to \frac{\mathbf{x}_i + \gamma \mathbf{F}_i^\tau}{\left|\mathbf{x}_i + \gamma \mathbf{F}_i^\tau\right|}, \tag{17}$$

where $\mathbf{F}_i^\tau$ is the component of $\mathbf{F}_i$ in the tangential direction and γ is a constant given by

$$\gamma = \frac{\beta a_0}{F_{\text{init}}^\tau}. \tag{18}$$

The largest tangential force in the starting configuration is given by F_{init}^τ and a_0 is a characteristic distance related to the number of particles and is approximately half the distance between particles for large N. The parameter β is user specified and here is chosen to be 0.5 based on several trial runs for smaller N.

Occasionally the algorithm will find configurations which are saddle points. Remarkably, this is a common occurrence for this problem (cf. [24,26,27]). The Hessian matrix in the neighborhood of these saddle points often has at least one small negative eigenvalue which slows the steepest descent procedure. In principle this can be solved by taking a larger descent step (choosing a larger β). However, the unstable directions are believed to be quite "narrow" such that the forces have only a small component along the unstable directions. If the optimization algorithm is continued (ignoring the stopping condition) then it eventually finds the local minimum; however doing so is inefficient. Instead, the putative optimal configurations are tested by computing the eigenvalues of the Hessian matrix and excluding those with negative eigenvalues. Note that the Hessian matrix is semidefinite at every local minima due to the rotational and reflectional invariance. Thus we fix the position of one particle and the azimuth of a second when computing the Hessian.

Due to the symmetry of the optimal configurations, many of the generated starting configurations, and putative minima, are identical up to rotation and reflection. Thus we require a method to distinguish configurations to avoid unnecessary computation and to avoid errors in counting the number of minima. In principle, one can simply compute the energy of each configuration using any "potential energy" function. However, for a given N the optimal energies are typically very similar (see Figs. 5 and 9 in the next two sections). When $N \leqslant 65$, this does not pose a problem (see Ref. [21]). As N increases it becomes more difficult to distinguish configurations using energy. Further, the energy is relatively insensitive to small changes in particle positions around local minima, making it difficult to resolve differences between two configurations.

Identifying equivalent configurations is accomplished with the set of $N(N-1)/2$ pairwise distances, which is invariant under rotation and reflection. Suppose we have K configurations; let $\mathbf{x}_i^{(k)}$ denote the ith particle in the kth configuration. The algorithm proceeds as follows:

(1) For each k, compute scalars $d_{ij}^k = |\mathbf{x}_i^{(k)} - \mathbf{x}_j^{(k)}|$, $i < j \leqslant N$, and let these be the components of $\mathbf{d}^{(k)}$.

(2) Sort $\mathbf{d}^{(k)}$ in ascending order and then normalize such that $\max_k(d_{ij}^{(k)}) = 1$ for a given i and j. Denote the resulting vector by $\tilde{\mathbf{d}}^{(k)}$.

(3) Compute the clustering tolerance

$$\delta = \frac{|\text{tol}|}{\max_k ||\tilde{\mathbf{d}}^{(k)}||_{L^2}}, \tag{19}$$

where tol is user specified and was chosen as 10^{-3} since this was found to give good results.

(4) Cluster the $\tilde{\mathbf{d}}^{(k)}$ using Euclidean distance (L^2 norm) and the tolerance in the previous step. This was implemented with the Statistics Toolbox in MATLAB. The authors note that using other distance metrics is possible; however we do not investigate this any further here.

All configurations within a cluster are identical up to rotation and reflection when an appropriate tolerance is chosen.

IV. RESULTS FOR THE NE POTENTIAL UP TO $N = 120$

Putative globally optimal configurations on the sphere for the NE potential have been computed for $N \leqslant 65$ in

TABLE I. List of global minima for the NE potential. In order, the columns show the number of particles, the NE globally optimal energy, and the number of local minima (including the global minimum).

N	NE Energy	No. of Local Minima	N	NE Energy	No. of Local Minima
4	−1.6671799	1	63	311.6558511	1
5	−2.0879876	1	64	324.0896299	1
6	−2.5810055	1	65	336.7697094	1
7	−2.7636584	1	66	349.6565931	2
8	−2.9495765	1	67	362.7514093	1
9	−2.9764336	1	68	376.2377825	3
10	−2.8357352	1	69	389.9300126	4
11	−2.4567341	1	70	403.8308809	5
12	−2.1612842	1	71	418.0224191	1
13	−1.3678269	1	72	432.3019807	4
14	−0.5525928	1	73	447.2100228	2
15	0.4774376	1	74	462.2113780	9
16	1.6784049	2	75	477.3635907	3
17	3.0751594	1	76	492.8366797	6
18	4.6651247	1	77	508.4749290	4
19	6.5461714	1	78	524.4487720	4
20	8.4817896	1	79	540.7371289	5
21	10.7013196	1	80	557.2315390	7
22	13.1017418	2	81	574.1035388	7
23	15.8212821	1	82	591.1522915	13
24	18.5819815	1	83	608.4133589	16
25	21.7249125	1	84	625.9597981	17
26	25.0100312	1	85	643.7723346	10
27	28.4296992	1	86	661.8438907	22
28	32.1929330	1	87	680.1575495	20
29	36.2197826	1	88	698.7043251	18
30	40.3544394	1	89	717.5605772	15
31	44.7576167	1	90	736.6531884	24
32	49.2409494	2	91	756.0230290	23
33	54.2959715	1	92	775.6539262	24
34	59.3794885	1	93	795.5664664	23
35	64.7367107	2	94	815.6923218	32
36	70.2760966	1	95	836.1253560	22
37	76.0662374	2	96	856.7795176	21
38	82.0802998	2	97	877.7410951	8
39	88.3295602	2	98	898.9117217	13
40	94.8178306	3	99	920.4235474	10
41	101.5685414	2	100	942.1286420	24
42	108.5402790	1	101	964.1753574	40
43	115.7702833	1	102	986.4289369	56
44	123.1634320	1	103	1008.9408904	41
45	130.9053156	1	104	1031.6959327	53
46	138.9204719	3	105	1054.8551489	58
47	147.1503518	5	106	1078.1682359	66
48	155.4174211	1	107	1101.7749883	54
49	164.2174643	1	108	1125.5711591	57
50	173.0786752	1	109	1149.7450890	82
51	182.2666362	2	110	1174.1102793	92
52	191.7242791	3	111	1198.7086529	60
53	201.3847501	2	112	1223.6244989	87
54	211.2834897	4	113	1248.8814345	93
55	221.4638138	6	114	1274.3559709	118
56	231.8539755	3	115	1300.0999781	124
57	242.5180260	4	116	1326.1250674	186
58	253.4345983	8	117	1352.3413825	232
59	264.5718539	4	118	1378.8765253	282
60	275.9094151	5	119	1405.6502758	254
61	287.6211392	6	120	1432.6666276	208
62	299.4803100	2			

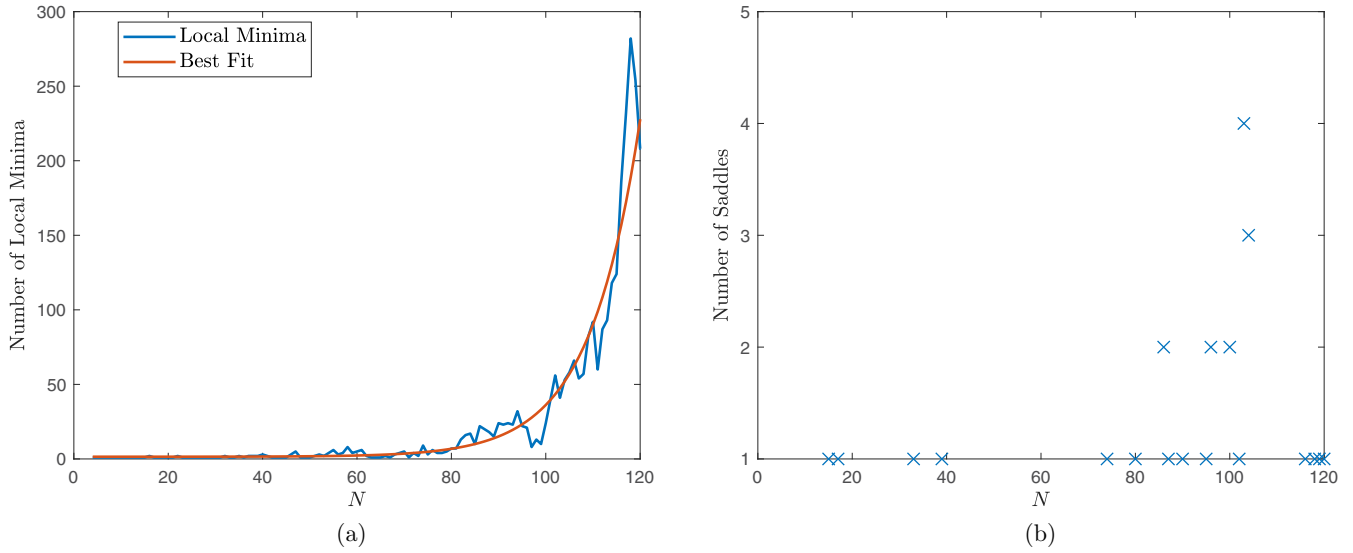

FIG. 4. (a) Number of minima found for the NE potential and the best-fit curve, Eq. (20). (b) Saddle points found for the NE potential.

Refs. [8,22]. In the latter study, globally optimal configurations for a few selected N up to 1004 were found. Locally optimal configurations have not previously been computed to the authors' knowledge. The current section is divided into three parts: First we present tables of the computed global minima and the corresponding energies. Then we give results for local minima, including energy spectra, tables up to $N = 65$, and scars. Finally, we compare the globally minimal energies with a previously derived asymptotic scaling law [8]. Data on the local minima for $N > 65$ are available in the Supplemental Material [29] but are not included here due to the amount of data.

A. Global minima

Table I gives the computed globally optimal energies for each N along with the number of computed local minima. Each configuration was verified by computing the eigenvalues of the Hessian matrix.

The computation time for each N increases rapidly due to the increase in local minima. The majority of the computation time was spent optimizing configurations for $115 \leqslant N \leqslant 120$ for which the number of starting configurations was between 25 000 and 66 000.

B. Local minima

The number of computed local minima for the NE potential is shown in Fig. 4. As the number of minima is expected to grow exponentially, we fit a curve of the form $a_0 + a_1 e^{a_2 N}$ in the least squares sense. This is a nonlinear curve fitting problem which is handled numerically with MATLAB's LSQCURVEFIT() function. We find

$$n(N) \approx 1.483278 + 0.002963 e^{0.093686N}, \tag{20}$$

where n is the best fit number of minima. The reasonable agreement supports the supposed exponential growth rate [6].

A total of 2780 putative minima and a few saddle points were discovered. A list of the local and global minima with their corresponding energies and geometric properties are given in Table II for $N \leqslant 65$. The remaining data for $N \leqslant 120$ are available in a MATLAB file in the Supplemental Material [29]. The computed energies are presented as a spectrum in Fig. 5. They become increasingly dense with N.

Computation of optimal configurations for the NE potential were also performed in Ref. [22]. We obtain slightly lower energies for $N = 90, 95$ and more significantly lower energies for $N = 105$ and $N = 115$. The other optimal energies agree with our results up to the given precision. Many of the energies obtained here are identical to those given in Table 4.2 of [8] to the given precision up to $N \approx 35$. Above $N \approx 35$ the energies given here are slightly lower.

Some examples of computed local minima are given in Fig. 6 showing the scar structure. In general, there appears to be little or no symmetry in this structure, especially for large N. As a general observation, coordination numbers alone do not provide enough information to distinguish configurations. This is also seen in the third and sixth columns of Table II in which many minima have the same coordination numbers for a given N. However, configurations with very different scar structures are likely not equivalent geometrically (as in Fig. 6).

C. A scaling law for the minimal NE energy

In this section, we compare the computed globally optimal energies with an asymptotic scaling law for the pairwise energy (7) valid in the limit $N \to \infty$. We rewrite Eq. (7) as

$$\mathcal{H}_{\mathrm{NE}} = \mathcal{H}_{\mathrm{C}} + \tfrac{1}{2}\mathcal{H}_{\mathrm{L}} + \mathcal{H}_{\mathrm{L2}}, \tag{21}$$

where $\mathcal{H}_{\mathrm{C}}$ and $\mathcal{H}_{\mathrm{L}}$ are given in Eqs. (8) and (9), respectively, and

$$\mathcal{H}_{\mathrm{L2}} = -\frac{1}{2}\sum_{i<j}^{N} \log(2 + |\mathbf{x}_i - \mathbf{x}_j|). \tag{22}$$

TABLE II. Comprehensive list of local and global minima for the NE potential (up to $N = 65$). In order, the columns show the number of particles, the NE energy, and the numbers of particles with coordination numbers 3 to 7. The remaining data up to $N = 120$ are available in the Supplemental Material [29].

N	NE Energy	$c_3 + c_4 + c_5 + c_6 + c_7$	N	NE Energy	$c_3 + c_4 + c_5 + c_6 + c_7$
4	−1.6671799	4+0+0+0+0		147.1833136	0+0+12+35+0
5	−2.0879876	2+3+0+0+0		147.2448260	0+0+12+35+0
6	−2.5810055	0+6+0+0+0	48	155.4174211	0+0+12+36+0
7	−2.7636584	0+5+2+0+0	49	164.2174643	0+0+12+37+0
8	−2.9495765	0+4+4+0+0	50	173.0786752	0+0+12+38+0
9	−2.9764336	0+3+6+0+0	51	182.2666362	0+0+12+39+0
10	−2.8357352	0+2+8+0+0		182.4052019	0+0+12+39+0
11	−2.4567341	0+2+8+1+0	52	191.7242791	0+0+12+40+0
12	−2.1612842	0+0+12+0+0		191.7276751	0+0+12+40+0
13	−1.3678269	0+1+10+2+0		191.7432297	0+0+12+40+0
14	−0.5525928	0+0+12+2+0	53	201.3847501	0+0+12+41+0
15	0.4774376	0+0+12+3+0		201.3952021	0+0+12+41+0
16	1.6784049	0+0+12+4+0	54	211.2834897	0+0+12+42+0
	1.6888964	0+0+12+4+0		211.2881597	0+0+12+42+0
17	3.0751594	0+0+12+5+0		211.2946443	0+0+12+42+0
18	4.6651247	0+2+8+8+0		211.2965687	0+0+12+42+0
19	6.5461714	0+0+12+7+0	55	221.4638138	0+0+12+43+0
20	8.4817896	0+0+12+8+0		221.4688811	0+0+14+39+2
21	10.7013196	0+1+10+10+0		221.4690985	0+0+12+43+0
22	13.1017418	0+0+12+10+0		221.4816551	0+0+12+43+0
	13.1259621	0+0+12+10+0		221.4821066	0+0+12+43+0
23	15.8212821	0+0+12+11+0		221.4948761	0+0+12+43+0
24	18.5819815	0+0+12+12+0	56	231.8539755	0+0+12+44+0
25	21.7249125	0+0+12+13+0		231.8541155	0+0+12+44+0
26	25.0100312	0+0+12+14+0		231.8581363	0+0+12+44+0
27	28.4296992	0+0+12+15+0	57	242.5180260	0+0+12+45+0
28	32.1929330	0+0+12+16+0		242.5606388	0+0+13+43+1
29	36.2197826	0+0+12+17+0		242.5722866	0+0+12+45+0
30	40.3544394	0+0+12+18+0		242.5742216	0+0+12+45+0
31	44.7576167	0+0+12+19+0	58	253.4345983	0+0+12+46+0
32	49.2409494	0+0+12+20+0		253.4429647	0+0+12+46+0
	49.4893595	0+0+12+20+0		253.4438456	0+0+12+46+0
33	54.2959715	0+0+13+19+1		253.4451075	0+0+12+46+0
34	59.3794885	0+0+12+22+0		253.4532446	0+0+12+46+0
35	64.7367107	0+0+12+23+0		253.4574482	0+0+12+46+0
	64.7405651	0+0+12+23+0		253.4675340	0+0+12+46+0
36	70.2760966	0+0+12+24+0		253.5691064	0+0+14+42+2
37	76.0662374	0+0+12+25+0	59	264.5718539	0+0+14+43+2
	76.0768682	0+0+12+25+0		264.5733388	0+0+12+47+0
38	82.0802998	0+0+12+26+0		264.5850623	0+0+12+47+0
	82.0931587	0+0+12+26+0		264.5916096	0+0+12+47+0
39	88.3295602	0+0+12+27+0	60	275.9094151	0+0+12+48+0
	88.3900685	0+0+12+27+0		275.9145551	0+0+12+48+0
40	94.8178306	0+0+12+28+0		275.9214751	0+0+12+48+0
	94.8756103	0+0+12+28+0		276.0688360	0+0+12+48+0
	94.8953050	0+0+12+28+0		276.0811919	0+0+12+48+0
41	101.5685414	0+0+12+29+0	61	287.6211392	0+0+12+49+0
	101.6395277	0+0+12+29+0		287.6322577	0+0+12+49+0
42	108.5402790	0+0+12+30+0		287.6359522	0+0+12+49+0
43	115.7702833	0+0+12+31+0		287.6534930	0+0+12+49+0
44	123.1634320	0+0+12+32+0		287.6561326	0+0+12+49+0
45	130.9053156	0+0+12+33+0		287.6655546	0+0+12+49+0
46	138.9204719	0+0+12+34+0	62	299.4803100	0+0+12+50+0
	138.9242053	0+0+12+34+0		299.5177575	0+0+12+50+0
	138.9260526	0+0+12+34+0	63	311.6558511	0+0+12+51+0
47	147.1503518	0+0+12+35+0	64	324.0896299	0+0+12+52+0
	147.1538854	0+0+12+35+0	65	336.7697094	0+0+12+53+0
	147.1659480	0+0+12+35+0			

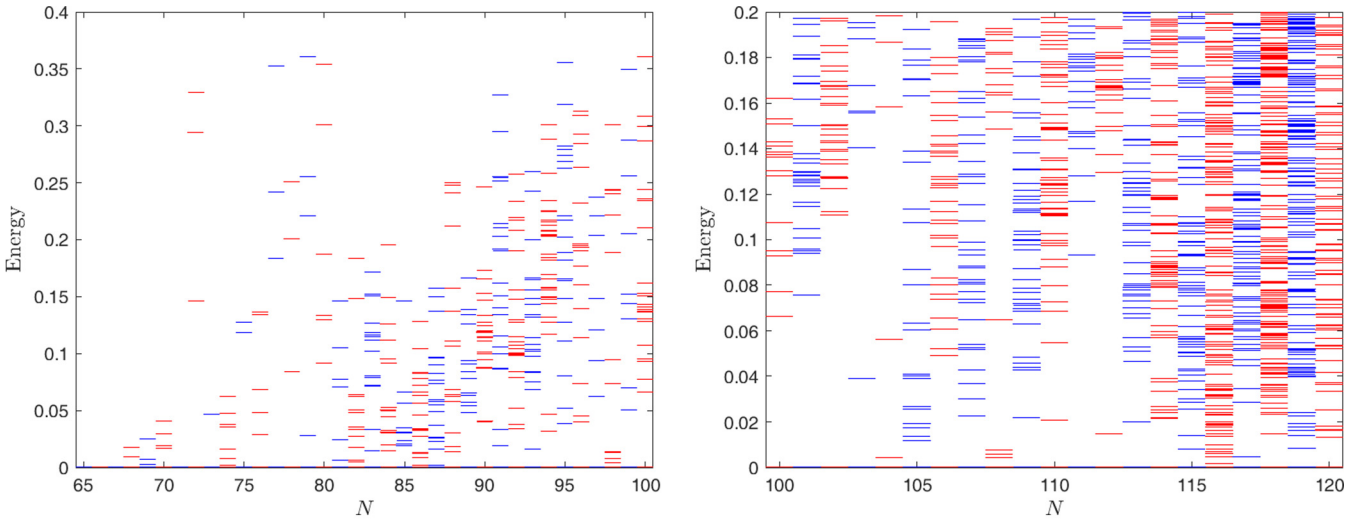

FIG. 5. NE energies of locally optimal configurations relative to the global minima for (a) $65 \leqslant N \leqslant 100$ and (b) $100 \leqslant N \leqslant 120$. The energies at zero correspond to the global minima. The vertical axes have been adjusted for clarity. Note that some minima fall outside the range of the vertical axis.

We have the following results from [8] [note the factor of $1/2$ difference in our definition of $\mathcal{H}_{\mathrm{L}}$, Eq. (9)]:

$$\mathcal{H}_{\mathrm{C}} \approx \frac{N^2}{2} - \frac{1}{2}N^{3/2} + \frac{1}{12}N^{1/2} + O(N^{-1/2}), \tag{23a}$$

$$\mathcal{H}_{\mathrm{L}} \approx \frac{N^2}{4}(1-2\log 2) - \frac{N}{4}\log N - \frac{N}{4}(1-2\log 2) + \frac{1}{12}\log N - \frac{1}{6}\log 2 + O(N^{-1}), \tag{23b}$$

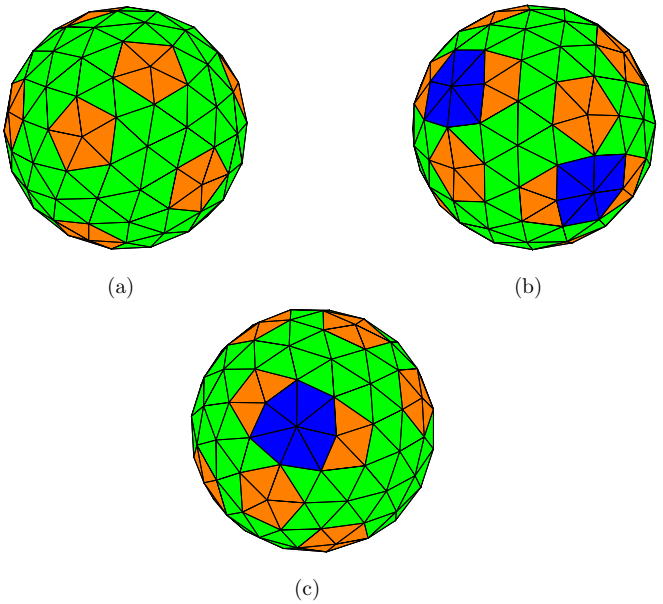

FIG. 6. Examples of optimal NE configurations for $N = 117$ for which 232 local minima were found. (a): The global minimum. (b) and (c): Two local minima adjacent in energy. The computed NE energies are approximately 1352.341, 1352.513, and 1352.514, respectively.

$$\mathcal{H}_{\mathrm{L2}} \approx -\frac{N^2}{8}(1+2\log 2) + \frac{\log 2}{4}N + \frac{1}{6}N^{1/2} - \left(\frac{1}{16} + \frac{\log 2}{12}\right) + O(N^{-1/2}). \tag{23c}$$

Substituting the above into (21) gives the desired scaling law (also derived in [8]):

$$\mathcal{H}_{\mathrm{NE}} \approx \frac{N^2}{2}(1-\log 2) - \frac{1}{2}N^{3/2} - \frac{N}{8}\log N - \frac{N}{8}(1-4\log 2) + \frac{1}{4}N^{1/2} + \frac{1}{24}\log N - \left(\frac{1}{16} + \frac{\log 2}{6}\right) + O(N^{-1/2}). \tag{24}$$

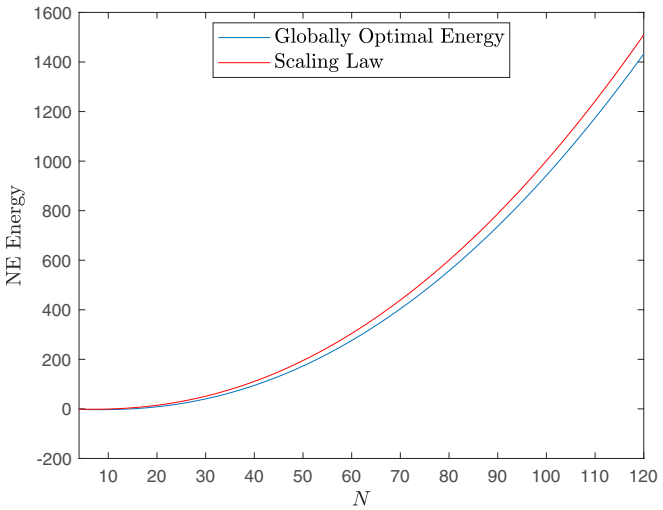

FIG. 7. Comparison of globally optimal NE energies with the asymptotic scaling law (24).

TABLE III. List of global minima for the NC potential. In order, the columns show the number of particles, the NC globally optimal energy, and the number of local minima.

N	Global NC Energy	Local Minima	N	Global NC Energy	Local Minima
4	1.2753079	1	63	761.7365139	1
5	2.3325195	1	64	787.7433643	1
6	3.6573191	1	65	814.1954515	1
7	5.4188195	1	66	841.0627048	2
8	7.4781865	1	67	868.3435424	1
9	9.9113144	1	68	896.1835478	3
10	12.7273233	1	69	924.4370909	4
11	15.9633917	1	70	953.1053374	5
12	19.4448610	1	71	982.2534837	2
13	23.4988136	1	72	1011.7220316	5
14	27.8546601	1	73	1041.9378711	3
15	32.6249857	1	74	1072.4773046	9
16	37.7841349	2	75	1103.3861677	3
17	43.3480585	1	76	1134.7989611	6
18	49.3152900	1	77	1166.5921261	4
19	55.7454616	1	78	1198.9012840	4
20	62.4925763	1	79	1231.7114783	5
21	69.7021610	1	80	1264.9343750	8
22	77.3074771	2	81	1298.7071786	7
23	85.3990644	1	82	1332.8686991	13
24	93.7956788	1	83	1367.4479328	16
25	102.7220631	1	84	1402.5044669	17
26	112.0190373	1	85	1438.0212839	10
27	121.6815612	1	86	1473.9935322	23
28	131.8513551	1	87	1510.4080648	21
29	142.4737389	1	88	1547.2565862	19
30	153.4431719	1	89	1584.6017630	19
31	164.8676908	1	90	1622.3838285	26
32	176.6198170	2	91	1660.6362010	24
33	189.0434647	1	92	1699.3452879	28
34	201.7545872	1	93	1738.5291591	27
35	214.9282924	2	94	1778.1304687	39
36	228.4996702	1	95	1818.2268735	24
37	242.5158012	2	96	1858.7481974	23
38	256.9600891	2	97	1899.7641064	11
39	271.8381200	2	98	1941.1954839	18
40	287.1550632	3	99	1983.1491796	14
41	302.9272985	2	100	2025.5050024	27
42	319.1244788	1	101	2068.3830362	41
43	335.7734900	1	102	2111.6744155	60
44	352.8052329	1	103	2155.4211861	50
45	370.3587315	1	104	2199.6110343	61
46	388.3757521	3	105	2244.3738904	63
47	406.8113090	5	106	2289.5077641	73
48	425.5351845	1	107	2335.1252008	60
49	444.9188072	1	108	2381.1411090	65
50	464.6065564	1	109	2427.7106073	94
51	484.7997393	2	110	2474.6800384	101
52	505.4557374	4	111	2522.0823797	75
53	526.5221776	2	112	2569.9899275	107
54	548.0282546	4	113	2618.4209072	111
55	570.0046269	6	114	2667.2735190	140
56	592.3987462	3	115	2716.5898475	159
57	615.2584023	5	116	2766.3811001	215
58	638.5661060	8	117	2816.5721460	265
59	662.2992461	4	118	2867.2673880	320
60	686.4417704	5	119	2918.4018751	284
61	711.1280295	6	120	2969.9778301	238
62	736.1836003	3			

TABLE IV. Comprehensive list of local and global minima for the NC potential up to $N = 65$. In order, the columns show the number of particles, the NC energy, and the numbers of particles with coordination numbers 3 to 7. The remaining data up to $N = 120$ are available in the Supplemental Material [29].

N	NC Energy	$c_3 + c_4 + c_5 + c_6 + c_7$	N	NC Energy	$c_3 + c_4 + c_5 + c_6 + c_7$
4	1.2753079	4+0+0+0+0		406.8826917	0+0+12+35+0
5	2.3325195	2+3+0+0+0	48	425.5351845	0+0+12+36+0
6	3.6573191	0+6+0+0+0	49	444.9188072	0+0+12+37+0
7	5.4188195	0+5+2+0+0	50	464.6065564	0+0+12+38+0
8	7.4781865	0+4+4+0+0	51	484.7997393	0+0+12+39+0
9	9.9113144	0+3+6+0+0		484.9059577	0+0+12+39+0
10	12.7273233	0+2+8+0+0	52	505.4557374	0+0+12+40+0
11	15.9633917	0+2+8+1+0		505.4584264	0+0+12+40+0
12	19.4448610	0+0+12+0+0		505.4705912	0+0+12+40+0
13	23.4988136	0+1+10+2+0		505.4723820	0+0+12+40+0
14	27.8546601	0+0+12+2+0	53	526.5221776	0+0+12+41+0
15	32.6249857	0+0+12+3+0		526.5304615	0+0+12+41+0
16	37.7841349	0+0+12+4+0	54	548.0282546	0+0+12+42+0
	37.7913424	0+0+12+4+0		548.0313595	0+0+12+42+0
17	43.3480585	0+0+12+5+0		548.0367702	0+0+12+42+0
18	49.3152900	0+2+8+8+0		548.0387819	0+0+12+42+0
19	55.7454616	0+0+12+7+0	55	570.0046269	0+0+12+43+0
20	62.4925763	0+0+12+8+0		570.0081782	0+0+12+43+0
21	69.7021610	0+1+10+10+0		570.0086879	0+0+14+39+2
22	77.3074771	0+0+12+10+0		570.0189717	0+0+12+43+0
	77.3248232	0+0+12+10+0		570.0192368	0+0+12+43+0
23	85.3990644	0+0+12+11+0		570.0289506	0+0+12+43+0
24	93.7956788	0+0+12+12+0	56	592.3987462	0+0+12+44+0
25	102.7220631	0+0+12+13+0		592.3992926	0+0+12+44+0
26	112.0190373	0+0+12+14+0		592.4021497	0+0+12+44+0
27	121.6815612	0+0+12+15+0	57	615.2584023	0+0+12+45+0
28	131.8513551	0+0+12+16+0		615.2702496	0+0+12+45+0
29	142.4737389	0+0+12+17+0		615.2905050	0+0+13+43+1
30	153.4431719	0+0+12+18+0		615.2995971	0+0+12+45+0
31	164.8676908	0+0+12+19+0		615.2996416	0+0+12+45+0
32	176.6198170	0+0+12+20+0	58	638.5661060	0+0+12+46+0
	176.7944252	0+0+12+20+0		638.5724213	0+0+12+46+0
33	189.0434647	0+0+13+19+1		638.5731306	0+0+12+46+0
34	201.7545872	0+0+12+22+0		638.5737991	0+0+12+46+0
35	214.9282924	0+0+12+23+0		638.5790228	0+0+12+46+0
	214.9315690	0+0+12+23+0		638.5834576	0+0+12+46+0
36	228.4996702	0+0+12+24+0		638.5846113	0+0+12+46+0
37	242.5158012	0+0+12+25+0		638.5919380	0+0+12+46+0
	242.5235820	0+0+12+25+0	59	662.2992461	0+0+14+43+2
38	256.9600891	0+0+12+26+0		662.2999789	0+0+12+47+0
	256.9687260	0+0+12+26+0		662.3091948	0+0+12+47+0
39	271.8381200	0+0+12+27+0		662.3147258	0+0+12+47+0
	271.8830066	0+0+12+27+0	60	686.4417704	0+0+12+48+0
40	287.1550632	0+0+12+28+0		686.4460598	0+0+12+48+0
	287.1986056	0+0+12+28+0		686.4520078	0+0+12+48+0
	287.2116587	0+0+12+28+0		686.5639093	0+0+12+48+0
41	302.9272985	0+0+12+29+0		686.5741767	0+0+12+48+0
	302.9816133	0+0+12+29+0	61	711.1280295	0+0+12+49+0
42	319.1244788	0+0+12+30+0		711.1365911	0+0+12+49+0
43	335.7734900	0+0+12+31+0		711.1399905	0+0+12+49+0
44	352.8052329	0+0+12+32+0		711.1533041	0+0+12+49+0
45	370.3587315	0+0+12+33+0		711.1553205	0+0+12+49+0
46	388.3757521	0+0+12+34+0		711.1624250	0+0+12+49+0
	388.3783317	0+0+12+34+0	62	736.1836003	0+0+12+50+0
	388.3791178	0+0+12+34+0		736.2003615	0+0+12+50+0

TABLE IV. (*Continued.*)

N	NC Energy	$c_3+c_4+c_5+c_6+c_7$	N	NC Energy	$c_3+c_4+c_5+c_6+c_7$
47	406.8113090	0+0+12+35+0		736.2121671	0+0+12+50+0
	406.8138763	0+0+12+35+0	63	761.7365139	0+0+12+51+0
	406.8222118	0+0+12+35+0	64	787.7433643	0+0+12+52+0
	406.8368865	0+0+12+35+0	65	814.1954515	0+0+12+53+0

Figure 7 compares the scaling law (24) with the computed globally optimal energies.

V. RESULTS FOR THE NC POTENTIAL UP TO $N = 120$

Optimal configurations (both local and global) for the NC potential have not previously been computed to the authors' knowledge. The current section is organized in the same way as the previous section. First we present tables of the computed global minima and the corresponding energies. Then we give results for local minima for $N \leqslant 65$ in a table, and finally we present a previously derived scaling law [14]. Data on the local minima for $N > 65$ cannot be included due to the amount of data and are available in the Supplemental Material [29].

A. Global minima

Table III gives the computed globally optimal energies for each N along with the number of computed local minima. As with the NE potential, the computation time grows rapidly with N. Between $N = 115$ and $N = 120$ the number of starting configurations grows from approximately 27 000 to 62 000, roughly the same as the NE potential.

B. Local minima

A total of 3170 putative minima and a few saddle points were found. A list of minima and corresponding geometric properties for $N \leqslant 65$ is given in Table IV. A complete list up to $N = 120$ is available in the Supplemental Material [29] in a MATLAB file.

As with the NE potential, we fit a curve of the form $n(N) = a_0 + a_1 e^{a_2 N}$ to the number of local minima, where n is the best fit number of minima. Using the same procedure as described in Sec. IV B, we find

$$n(N) \approx 2.968630 + 0.000376 e^{0.113313N}. \tag{25}$$

Figure 8 shows the number of optimal configurations before and after removal of saddle points along with the best fit curve (25).

A spectrum plot of the locally optimal energies is given in Fig. 9. The minima become increasingly dense as N increases. Figure 10 shows examples of computed local minima and their scar structure.

C. A scaling law for the minimal NC energy

We compare the computed globally optimal energies for the NC potential with an asymptotic scaling law for Eq. (14) valid in the limit $N \to \infty$. Using the same procedure as in Sec. IV C, we write the NC energy as

$$\mathcal{H}_{\mathrm{NC}} = \mathcal{H}_{\mathrm{C}} - \tfrac{1}{2}\mathcal{H}_{\mathrm{L}} + \mathcal{H}_{\mathrm{L2}}, \tag{26}$$

where $\mathcal{H}_{\mathrm{C}}$, $\mathcal{H}_{\mathrm{L}}$, and $\mathcal{H}_{\mathrm{L2}}$ are defined in Eqs. (8), (9), and (22), respectively. Substituting Eqs. (23a)–(23c) into the above yields the scaling law (also derived in [14])

$$\mathcal{H}_{\mathrm{NC}} \approx \frac{N^2}{4} - \frac{1}{2}N^{3/2} + \frac{N}{8}\log N + \frac{N}{8} + \frac{1}{4}N^{1/2} - \frac{1}{24}\log N - \frac{1}{16} + O(N^{-1/2}). \tag{27}$$

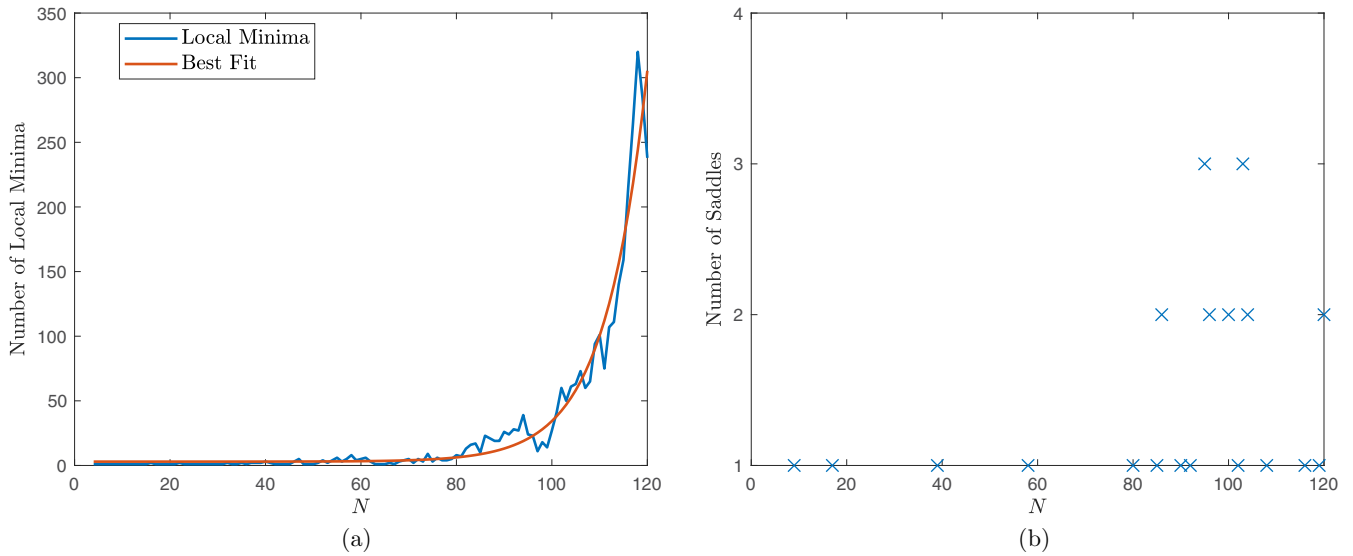

FIG. 8. (a) Number of minima found for the NC potential and the best-fit curve, Eq. (25). (b) Saddle points found for the NC potential.

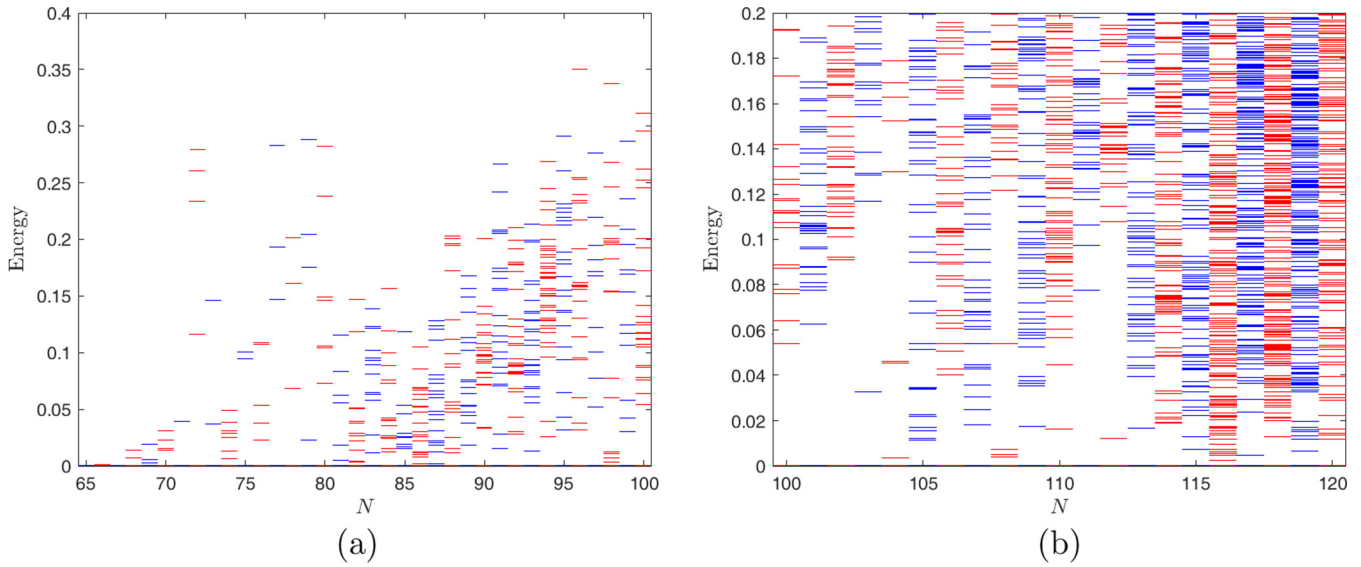

FIG. 9. NC energies of locally optimal configurations relative to the global minima for (a) $65 \leqslant N \leqslant 100$ and (b) $100 \leqslant N \leqslant 120$. The energies at zero correspond to the global minima. The vertical axes have been adjusted for clarity. Note that some minima fall outside the range of the vertical axis.

Figure 11 compares the scaling law (27) with the computed globally optimal energies.

VI. DISCUSSION

In [21], putatively optimal configurations for the Coulombic, logarithmic, and inverse square law potentials were computed for $N \leqslant 65$. Nonoptimal saddle points were excluded by computing the eigenvalues of the Hessian matrix. The discovered minima were compared with previous literature [24,26,27] and it was found that nearly all of the optimal configurations were reproduced and that some of the previously identified minima are indeed saddle points. Here, we used the same method to compute putatively optimal configurations of the narrow escape and narrow capture potentials for $N \leqslant 120$.

It is interesting that many of the local minima for all five of these potentials look qualitatively similar with respect to their scar pictures. We compared local minima across these potentials to determine if any are identical. The configurations that are shared among these potentials are termed *partially optimal* and these include the universal optima. Following Sec. III, we used pairwise distances to identify partially

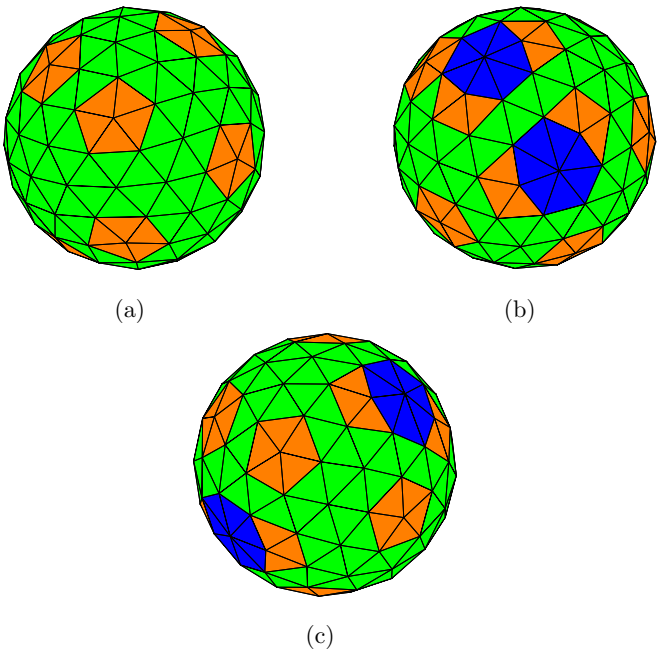

FIG. 10. Examples of optimal NC configurations for $N = 120$ for which 238 local minima were found. (a): The global minimum. (b) and (c): Two local minima adjacent in energy. The computed NC energies are approximately 2969.978, 2970.301, and 2970.304, respectively.

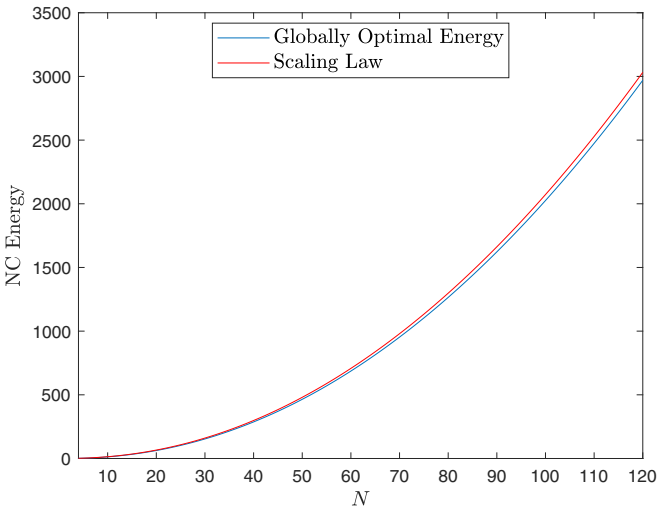

FIG. 11. Comparison of globally optimal NC energies with the asymptotic scaling law (27).

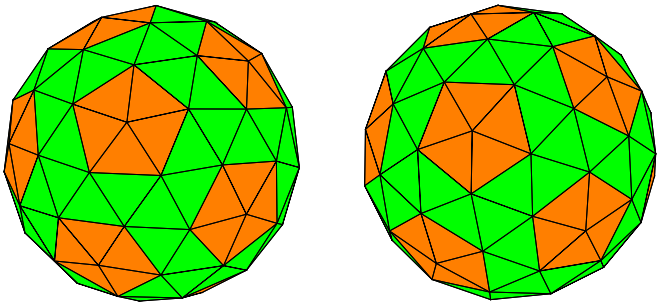

(a) (b)

FIG. 12. Global minima for the NC (a) and NE (b) potentials for $N = 72$ that appear close to being partially optimal. For these configurations, we compute $\alpha \approx 8.67 \times 10^{-3}$.

optimal configurations; i.e., for a given N we computed

$$\alpha(k_1, k_2) \equiv ||\tilde{\mathbf{d}}^{(k_1)} - \tilde{\mathbf{d}}^{(k_2)}||_{L^2} \tag{28}$$

for configurations indexed by k_1 and k_2 that come from different potentials. Here $\tilde{\mathbf{d}}^{(k)}$ is defined above (19). Note that $\alpha \sim 10^{-1}$ for geometrically different configurations. For the $N = 32$ global minima we found that $\alpha \sim 10^{-11}$ for each pair of potentials, indicating that the configurations are identical and therefore partially optimal. We also found that $\alpha \sim 10^{-13}$ for the $N = 7$ global minima with the exception of the logarithmic and inverse power law potentials for which $\alpha \sim 10^{-5}$. This indicates that the $N = 7$ global minimum may be partially optimal as well. There are other N for which the configurations are close but do not appear partially optimal (e.g., when $N \lesssim 20$ and $N = 72$ as shown in Fig. 12).

The $N = 32$ global minimum is in a special class of icosadeltahedral configurations that occur when

$$N = n^2 + nm + m^2 + 2, \qquad n, m \in \mathbb{Z}_+. \tag{29}$$

These configurations have 12 pentagonal defects arranged at the vertices of an inscribed icosahedron. It was once believed that this class of configurations was universally optimal; however this is not the case despite the high degree of symmetry for these configurations [30]. The next of these arrangements occurs at $N = 72$ and both the narrow escape and narrow capture potentials exhibit global minima with apparent icosadeltahedral symmetry upon visual inspection. However, the difference in pairwise distances indicate that these configurations are in fact different. The scar structure alone is not enough to distinguish configurations since different minima for a given N typically have identical coordination numbers.

In future work it may be of practical interest to apply results from the narrow escape problem to modeling diffusion in inverse opals. The "dwell time" (i.e., MFPT) of a diffusing particle in a single spherical cavity may be important for understanding diffusion in a connected network of such cavities. Inverse opals have been studied experimentally and numerically (e.g., Ref. [18]), but developing a quantitative theory of diffusion is still an open problem.

ACKNOWLEDGMENT

The authors are grateful to the Natural Sciences and Engineering Research Council of Canada (NSERC) for support through a Discovery Grant No. RGPIN-2014-05733, and also for support through a USRA fellowship.

[1] M. J. Bowick and L. Giomi, Two-dimensional matter: Order, curvature and defects, Adv. Phys. **58**, 449 (2009).

[2] J. D. Pintér, *Global Optimization in Action: Continuous and Lipschitz Optimization: Algorithms, Implementations and Applications* (Springer US, New York, 2013).

[3] R. Horst and P. M. Pardalos, *Handbook of Global Optimization* (Springer US, New York, 2013), Vol. 2.

[4] L. Davis, *Handbook of Genetic Algorithms* (Van Nostrand Reinhold, New York, 1991).

[5] L. Ingber and B. Rosen, Genetic algorithms and very fast simulated reannealing: A comparison, Math. Comput. Model. **16**, 87 (1992).

[6] D. Mehta, J. Chen, D. Z. Chen, H. Kusumaatmaja, and D. J. Wales, Kinetic Transition Networks for the Thomson Problem and Smale's Seventh Problem, Phys. Rev. Lett. **117**, 028301 (2016).

[7] S. Pillay, M. J. Ward, A. Peirce, and T. Kolokolnikov, An asymptotic analysis of the mean first passage time for narrow escape problems: Part I: Two-dimensional domains, Multiscale Model. Simul. **8**, 803 (2010).

[8] A. F. Cheviakov, M. J. Ward, and R. Straube, An asymptotic analysis of the mean first passage time for narrow escape problems. Part II. The sphere, Multiscale Model. Simul. **8**, 836 (2010).

[9] M. V. Keldysh and L. I. Sedov, Effective solution of some boundary-value problems for harmonic functions, Dokl. Akad. Nauk SSSR **16**, 7 (1937).

[10] M. Lavrentiev and B. Shabat, *Methods of Complex Function Theory* (Nauka, Moscow, 1987) (in Russian).

[11] Z. Schuss, A. Singer, and D. Holcman, The narrow escape problem for diffusion in cellular microdomains, Proc. Natl. Acad. Sci. USA **104**, 16098 (2007).

[12] Z. Schuss, *Brownian Dynamics at Boundaries and Interfaces* (Springer-Verlag, New York, 2015).

[13] A. E. Lindsay, T. Kolokolnikov, and J. C. Tzou, Narrow escape problem with a mixed trap and the effect of orientation, Phys. Rev. E **91**, 032111 (2015).

[14] A. E. Lindsay, A. J. Bernoff, and M. J. Ward, First passage statistics for the capture of a Brownian particle by a structured spherical target with multiple surface traps, Multiscale Model. Simul. **15**, 74 (2017).

[15] A. F. Cheviakov and M. J. Ward, Optimizing the principal eigenvalue of the Laplacian in a sphere with interior traps, Math. Comput. Model. **53**, 1394 (2011).

[16] R. Raccis, A. Nikoubashman, M. Retsch, U. Jonas, K. Koynov, H.-J. Butt, C. N. Likos, and G. Fytas, Confined diffusion in periodic porous nanostructures, ACS Nano **5**, 4607 (2011).

[17] M. J. Skaug and D. K. Schwartz, Tracking nanoparticle diffusion in porous filtration media, Ind. Eng. Chem. Res. **54**, 4414 (2015).

[18] T. Cherdhirankorn, M. Retsch, U. Jonas, H.-J. Butt, and K. Koynov, Tracer diffusion in silica inverse opals, Langmuir **26**, 10141 (2010).

[19] H. Cohn and A. Kumar, Universally optimal distribution of points on spheres, J. Am. Math. Soc. **20**, 99 (2007).

[20] B. Ballinger, G. Blekherman, H. Cohn, N. Giansiracusa, E. Kelly, and A. Schürmann, Experimental study of energy-minimizing point configurations on spheres, Exp. Math. **18**, 257 (2009).

[21] W. J. Ridgway and A. F. Cheviakov, An iterative procedure for finding locally and globally optimal arrangements of particles on the unit sphere, Comput. Phys. Commun. **233**, 84 (2018).

[22] A. F. Cheviakov and D. Zawada, Narrow-escape problem for the unit sphere: Homogenization limit, optimal arrangements of large numbers of traps, and the n^2 conjecture, Phys. Rev. E **87**, 042118 (2013).

[23] A. F. Cheviakov, A. S. Reimer, and M. J. Ward, Mathematical modeling and numerical computation of narrow escape problems, Phys. Rev. E **85**, 021131 (2012).

[24] T. Erber and G. M. Hockney, Equilibrium configurations of N equal charges on a sphere, J. Phys. A **24**, L1369 (1991).

[25] T. Erber and G. M. Hockney, Comment on Method of Constrained Global Optimization, Phys. Rev. Lett. **74**, 1482 (1995).

[26] T. Erber and G. M. Hockney, Complex systems: Equilibrium configurations of N equal charges on a sphere ($2 \leqslant N \leqslant 112$), Adv. Chem. Phys. **98**, 495 (1997).

[27] B. Bergersen, D. Boal, and P. Palffy-Muhoray, Equilibrium configurations of particles on a sphere: The case of logarithmic interactions, J. Phys. A **27**, 2579 (1994).

[28] W. Guo, D. Jin, and H. J. Maris, Theory of the stability of multielectron bubbles in liquid helium, J. Phys.: Conf. Ser. **150**, 032027 (2009).

[29] See Supplemental Material at http://link.aps.org/supplemental/10.1103/PhysRevE.100.042413 for the full computational results and datasets.

[30] E. L. Altschuler, T. J. Williams, E. R. Ratner, R. Tipton, R. Stong, F. Dowla, and F. Wooten, Possible Global Minimum Lattice Configurations for Thomson's Problem of Charges on a Sphere, Phys. Rev. Lett. **78**, 2681 (1997).